Astron. Astrophys. 336, 359–366 (1998)

ASTRONOMY AND ASTROPHYSICS

The study of magnetic field configuration of a 1N/M1.1 flare in AR7321

Wang Tongjiang[1], **Qiu Jiong**[2], **and Zhang Hongqi**[1]

[1] Beijing Astronomical Observatory, Chinese Academy of Sciences, Beijing 100080, P.R. China (e-mail: wtj@sun10.bao.ac.cn)
[2] Department of Astronomy, Nanjing University, Nanjing 210093, P.R. China

Received 30 September 1997 / Accepted 30 April 1998

Abstract. The present paper is aimed at reconstructing the magnetic configuration in an active region. The temporal evolution and spatial correlation of the magnetic features deduced from the photospheric observations have been investigated. Specifically, we have studied the non-potentiality in terms of new emerging flux, the vertical current system inferred from the photospheric vector magnetograms, and the distribution of magnetic free energy in the active region. We include a comparison between the magnetic connectivity patterns and the multi-waveband observations of a 1N/M1.1 flare in order to recover a comprehensive configuration from the photosphere up to the corona. The major results of this paper are: 1. the magnetic flux emergence considerably complicates the magnetic field with strong shear and enhancement of the vertical current system on the eve of the occurrence of the 1N/M1.1 flare. 2. The emerging bipole and some other pre-existing magnetic connection patterns, discovered from the photospheric observation, are identified with the flaring loops observed in the chromosphere and corona. 3. The footpoints of the flaring loops are located around the vertical current concentrations, indicating that they are perhaps current-carrying loops. 4. The emerging small loop interacts with the nearly paralell overlying long loop, which initiates the onset of the flare. Further energy release is triggered along the small loop, especially at the two foot regions, where the magnetic free energy is concentrated.

Key words: Sun: activity – Sun: flares – Sun: magnetic fields

1. Introduction

It is commonly accepted that the energetic phenomenon of flares results from the release of free energy stored in the non-potential magnetic field. The formation of non-potential field configuration is usually associated with flux emergence (Zirin 1983; Zhang 1995; Lites et al. 1995), during which, two kinds of shear can be present. In the first case, the strong shear is concentrated on the boundary of two bipoles, where the new emerging one collides with the old one to form a δ-structure; it is suggested that the boundary of such δ-structures characterizes the intersection of separatrices with the photosphere (Shi & Wang 1994; Shi et al. 1995). In the second case, new bipoles are born carrying the shear already in the emergence (Tanaka 1991; Wang & Tang 1993). The former case may infer the interaction of emerging magnetic loops, while the latter case seems to mean that the non-potential energy in magnetic loops probably pre-exists before they emerge from below the photosphere.

When a complex non-potential field is developed, the pre-existing and emerging magnetic loops may form a current-carrying system (Wang, Xu, & Zhang 1994; Leka et al. 1996). It is argued that the interaction between current-carrying magnetic loops makes an essential ingredient in trigger of the high-power energy release (Machado et al. 1988; Leka et al. 1993; Zhang & Wang 1994). Based on the evolution of vector magnetograms, Wang, Xu, & Zhang (1994) found that a large-scale new current system was established with an emerging bipole, and a series of flares were powered when it interacted with the old current system. Such scenario of flares was also found in the morphological analysis of SXR loops from *Yohkoh* observations (Kurokawa et al. 1992; Akioka et al. 1993; Hanaoka 1996).

From the observational point of view, the association between the magnetic configuration and flares are getting more and more confirmed. In some studies, the spatial correlation between the flare location and the topological features of the active region have been demonstrated (Démoulin, Hénoux & Mandrini 1992; Démoulin et al. 1994; Mandrini et al. 1993, 1995, 1996). On the other hand, the traditionally defined non-potential properties, like magnetic shear and vertical current system, deduced from the analysis of photospheric vector magnetograms, are observed to be spatially correlated with H_α or H_β flare kernels (Hagyard & Rabin 1986; Moore, Hagyard, & Davis 1987; Hagyard 1990; Canfield et al. 1993; Wang, Xu, & Zhang 1994; Fontenla et al. 1995; Wang et al. 1996). Knowledge of the spatial configuration of a magnetic field is an important clue to the understanding of such a relationship and of the mechanism of energy release (Priest 1981; Machado et al. 1988). However, the present instrumental capabilities are not able to observe directly the comprehensive magnetic field in the whole space but only magnetograms in the photosphere are available; instead, the coaligned multi-waveband observations offer an indirect way to access this problem. In a previous paper (Qiu et al. 1997; hereafter Paper I), we have studied in detail a

Send offprint requests to: T. Wang

flare event in AR7321, observed in chromospheric and coronal emissions, and investigated the thermal and nonthermal features involved in this event. Such a study of the co-ordinated data from the chromosphere to the corona, with very high spatiotemporal resolutions to date, also provides the opportunity to explore the possibility to recover the magnetic configuration where the flare occurred and was fueled. In this context, in the present paper, we will concentrate on the fact that the active region for this flare is a typical emerging flux region (EFR), where strong emerging flux pronouncedly changed the magnetic field from a simple bipole structure into a complex field with multiple magnetic loops (Liu et al. 1998; Wang, Wang, & Qiu 1997).

In the following, we will describe the instrumentation and observation of HSOS magnetic field in Sect. 2. In Sects. 3 and 4, the evolutions of the vector magnetic field and vertical current system are presented respectively, which, in Sect. 5, are further compared with the flare in term of their spatial relationships. In Sect. 6, we discuss the scenario of the flare in the light of the understanding on the configuration obtained in the previous sections. We come to the conclusion in the last section.

2. Observation

The active region NOAA7321 was an emerging flux region (EFR), which was born on October 24, 1992 and disappeared from the western limb on November 2. During the few days, it underwent a continuous change in configuration and frequent flares haunted this region. Preliminary studies on the magnetic features and flares in this active region have been published (Kawakami 1993; Takakura et al. 1994; Zhang 1995) and in the present paper we will investigate in detail the evolution of the magnetic configuration from October 26 to October 27 as a clue to the interpretation of the 1N/M1.1 flare at 01:44UT on October 27.

The flare at 01:44UT on October 27 was observed by the H_α spectrometer in the solar tower in Nanjing University and the *Yohkoh* instruments SXT, HXT and BCS. The flare underwent the onset, impulsive phase and the decaying phase, evolving rapidly within half an hour. It was made up of a low-lying, compact flaring loop with its two feet emitting intensely in both HXR and H_α bands, and some other coronal bright structures (loops). The analysis of the co-ordinated observations was done by Qiu et al. (1997 Paper I). In Sects. 5 and 6, we will refer to some of the main results in Paper I for further investigation in this paper.

For this active region, a series of photospheric vector magnetograms (FeI 5324.19Å) and H_β filtergrams (4861.34Å) were taken by the Solar Magnetic Field Telescope (SMFT) in Huairou Solar Observing Station (HSOS), Beijing Astronomical Observatory. The field of view is $5'.23 \times 3'.63$, and the angular resolution is around $2'' \times 2''$. The noise level of the line-of-sight magnetograms is < 25G, while for the transverse magnetograms, it is less than 190G, estimated from the average value of the transverse field strength in areas far away from flux concentrations in the active region. The 180° ambiguity in the transverse field is resolved by using the empirical method in a multi-step procedure (Canfield et al. 1993; Wang 1994).

3. Evolution of magnetic configuration

From Oct. 26 to Oct. 27, considerable changes were taking place in the magnetic configuration, which was characterized by the emerging flux and the motions of spots. Two vector magnetograms on Oct. 26 and 27 are compared in Fig. 1; the latter was taken just before the onset of the 01:44UT flare. Seen in the figure, the major spots N and S were present and made the main poles in the active region. East to the N spot, a group of satellite spots made up the S2 polarity. The inversion line of the line-of-sight field is drawn. For convenience, we name the segment of the inversion line that separates N from S as M1 and the segment separating N from S2 as M2.

On Oct. 26 (Fig. 1a), due to the emerging flux along the inversion line, the non-potential feature was already strong in the active region, as manifested by the transverse field which was almost aligned with the inversion line. The shear angle thus defined by Hagyard et al. (1984) was near 90° along both M1 and M2. The alignment of transverse field lines also defines the magnetic connectivity in this region, which was roughly divided into two patterns by M1. The first pattern, labeled as L1 in Fig. 1a, connected the minor spots of N1 and S1 and the second pattern L2 connected N' with S2. It is distinctive that emerging flux along the inversion line made up the connectivity patterns in this region. The connectivity patterns shown in Fig. 1 are plotted by tracing the vector of transverse field lines. They can be supposed as magnetic loops projected on the photosphere (Liu et al. 1998; Wang et al. 1997), which, in Sect. 5, will be further confirmed by the comparison with the flare configuration in space.

The emerging flux system was fully developed on Oct. 27 (Fig. 1b). Compared with the magnetogram taken one day before, several new spots, N3, S3, and S4 appeared, and N1 were enhanced evidently. The emerging magnetic structures brought in new connectivity patterns as well. Seen in Fig. 1b, the alignment of the transverse field along M1 was changed, perhaps due to the appearance of a new pattern L3 (drawn by hand in thick white lines in the figure), which connected N3 with S3. With the emergence of L3, the shape of M1 was different from one day before and the spots N and N1 were pushed southwest. As a result, L1 was twisted and the magnetic structure of the spot N rotated clockwisely by an angle of about 20°. For the pattern L2, not much change was taking place and the magnetic shear here remained high, but the spots of S2 group showed a running-away motion. Besides, between N1 and S4, yet another pattern L4 was formed, which was not seen one day before.

4. Vertical current system

The non-potential feature of the magnetic field, specifically, the strong shear of transverse field along the inversion line, implies that the active region could well be a current-carrying system, which was formed by emerging flux and spots motions. In this

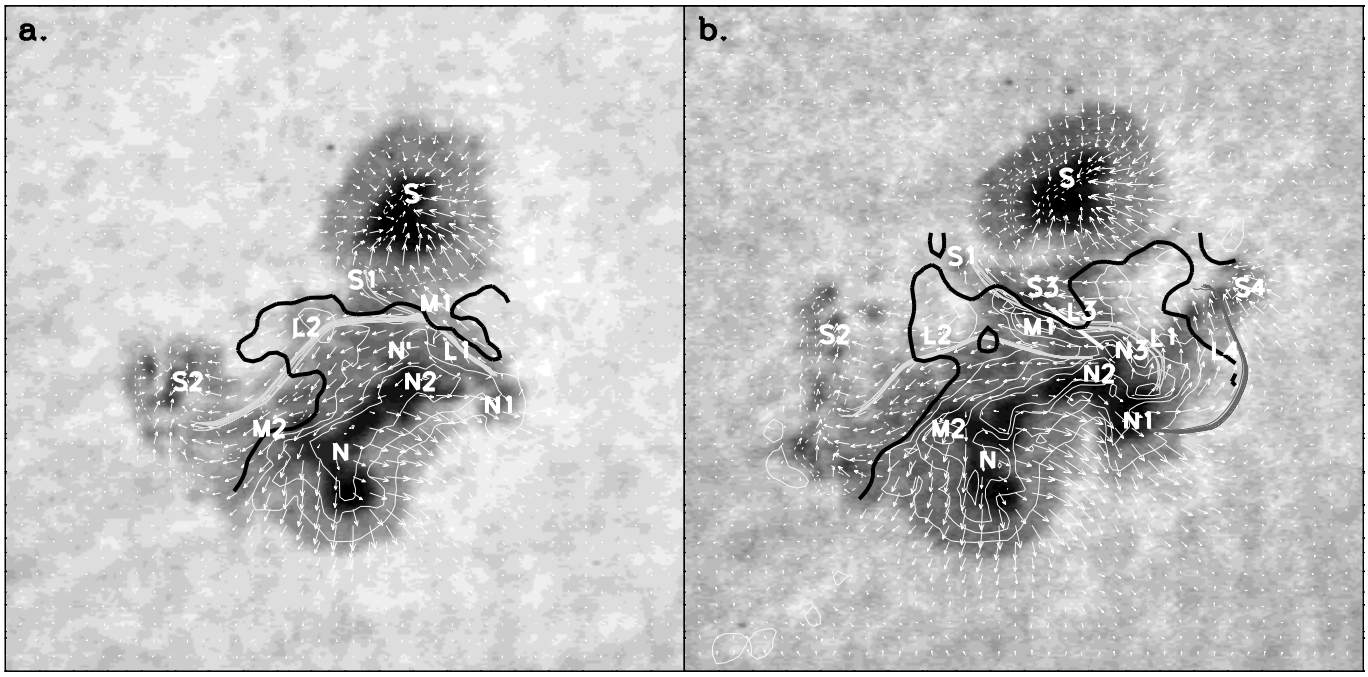

Fig. 1a and b. The photospheric vector magnetograms (contours) taken on **a** Oct. 26, 03:34UT and **b** Oct. 27, 01:44UT superposed on the white light images showing the spots. The white contours in both figures demonstrate the intensity of the longitudinal field (levels = ±500, 1500, 2500, and 3500 Gauss); solid lines show positive field and dashed lines show the negative field. The short arrows indicate the transverse field; the length of each arrow gives the magnitude of the field and the arrow gives the direction. The longitudinal inversion line is plotted in thick dark lines and the grey, thick curves indicate the magnetic connection patterns and the white straight segment drawn by hand indicate L3 (see the text). The field of view (FOV) is $170'' \times 170''$.

section, we will examine the evolution of the major vertical current channels (regions of high vertical current density) from October 26 to October 27.

4.1. Distribution of vertical current

In order to calculate the vertical current, we first pretreat the transverse field data with a Fourier low-pass filter. This method is proved efficient for minimizing the high-frequency measurement noises without losing the major structures in the field (Wang et al. 1997). Hence the vertical current can be readily deduced with the differencing method and the accuracy of such calculation is directly determined by the resolution of the filter. For our data, we obtain the filtering resolution as about $11'' \times 7''$, when the relative cutoff frequency, $\bar{k_c}$, is given as 15. $\bar{k_c}$ is a dimensionless quantity normalized to $2\pi\sqrt{1/L_x^2 + 1/L_y^2}$, where L_x and L_y are the characteristic sizes of the active region. The major vertical current channels can be illustrated in this resolution (Fig. 2) and the noise level in the vertical current is estimated from the standard deviation of currents measured in areas where the transverse field is weak (Canfield et al. 1993).

Fig. 2 shows the distributions of the vertical current density in gray-scale maps with the contours of the line-of-sight magnetograms superposed on. The vertical currents above the $2\sigma_J$ level are drawn in the maps. The current upflowing from the photosphere (the positive footpoint) is shown in bright colors, while that flowing down into the photosphere (the negative footpoint) is shown in dark colors.

In order to check the balance between the upflowing and downflowing currents, in Table 1, we list and compare the total positive/negative vertical current I^+/I^- calculated at different current cutoff levels (J_c=σ_J, $2\sigma_J$, and $3\sigma_J$). The minimum and maximum vertical current densities J_{min} and J_{max} are also given in Table 1. From the imbalance measurement $\Delta I/\bar{I}$ (defined as $2(I^+ - I^-)/(I^+ + I^-)$), it is seen that the total currents are basically balanced when the cutoff J_c is taken as σ_J, or $2\sigma_J$, whereas the upflowing current dominates in the active region when the cutoff is taken as $3\sigma_J$; this is especially true on October 27, when the imbalance measurement exceeds 22%. This can be understood with respect to the fact that the upflowing current is strong and concentrated, while the downflowing current is relatively weak and disperse, and this trend becomes more obvious on October 27. The distinct imbalance of the total currents at $3\sigma_J$ level also means that this selection of the current cutoff value is probably unsuitable for this active region.

4.2. Evolution of the vertical current system

On October 26 (Fig. 2a), the pair of current footpoints J_1^+ and J_{11}^--J_{12}^- were just located along the zone of the emerging pattern L1, and J_1^+, J_{12}^- were co-spatial with the emerging poles N1 and S1, implying that L1 might be a current-carrying pattern. Similarly, the dominant current pair J_2^+ and J_2^- were also located

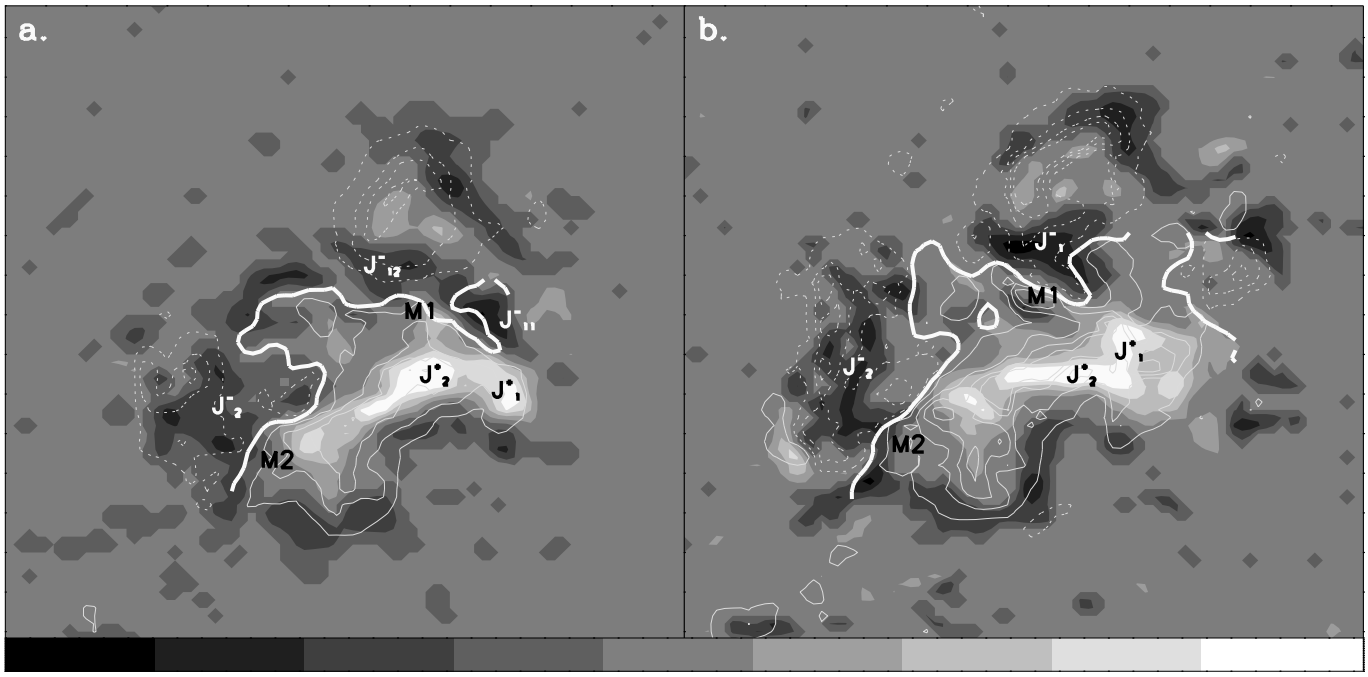

Fig. 2a and b. Vertical current distributions on **a** Oct. 26 and **b** Oct. 27 with the magnetic longitudinal field superposed on (solid and dashed contours). The bright (dark) color indicate the current flowing out of (into) the photosphere, or upward (downward). The grey scale at the bottom gives the intensity of the current and the levels are -2.4, -1.8, -1.2, -0.6, 0, 0.6, 1.2, 1.8, 2.4×10^{-2}A/m^2 from dark to bright colors. The magnetic longitudinal inversion line is drawn in white, thick lines in both figures. The FOV is the same as that in Fig. 1.

Table 1. Parameters of the vertical current distribution

Cutoff of current density J_c	October 26			October 27		
	σ_J	$2\sigma_J$	$3\sigma_J$	σ_J	$2\sigma_J$	$3\sigma_J$
Positive total current I^+ (10^{13}A)	2.34	1.52	1.18	3.59	2.01	1.43
Negative total current I^- (10^{13}A)	2.35	1.51	1.13	3.55	1.91	1.15
Current imbalance measurement $\Delta I/\bar{I}$ (%)	−0.31	0.22	4.4	1.0	5.0	22.
Noise level of current σ_J (mA/m^2)		1.3			2.4	
Minimum current density J_{min} (mA/m^2)		−19			−23	
Maximum current density J_{max} (mA/m^2)		34			35	

in the area where the dominant emerging pattern L2 was present and the maximum of positive current footpoint J_2^+ was co-spatial with the pole N2, the most drastic emerging feature on this day.

On October 27 (Fig. 2b), the total currents increased with the enhancement of the emerging poles. The current pair J_1^+-J_1^- became significant. The positive footpoint J_1^+ extended to a larger area and its maximum turned to be associated with the newly emerging pole N3; on the other hand, the negative footpoints J_{12}^- became more stronger (addressed as J_1^- in the figure) while J_{12}^- disappeared. Such change was associated with the enhanced pole S1 and the new pole S3. Due to the motions of the dominant emerging poles, there was some change in the morphology of the current pair J_2^+-J_2^-. In addition, it is noteworthy that the sections M1 and M2 of the magnetic inversion line were nearly coincident with the reverse lines of the vertical currents, and the vertical current density bore a strong gradient on both sides of the current reverse lines.

The analysis of the vertical current system reveals the following features in its evolution: (1) the major current pairs are associated with the dominant emerging patterns; (2) the peak of the current footpoints appears to be nearly located in the areas with the most drastically emerging poles; and (3) the sections of the magnetic inversion line are coaligned with the current reverse lines, where there is a strong vertical current gradient and perhaps horizontal currents.

5. Spatial correlation between the flare and magnetic configuration

5.1. Flare identity of the magnetic loops

The 1N/M1.1 flare occurred at 01:44UT on October 27. A comprehensive study of the coordinated observations of the event was given in Paper I. From the observations, the configuration of the flare from the low chromosphere up to the corona can

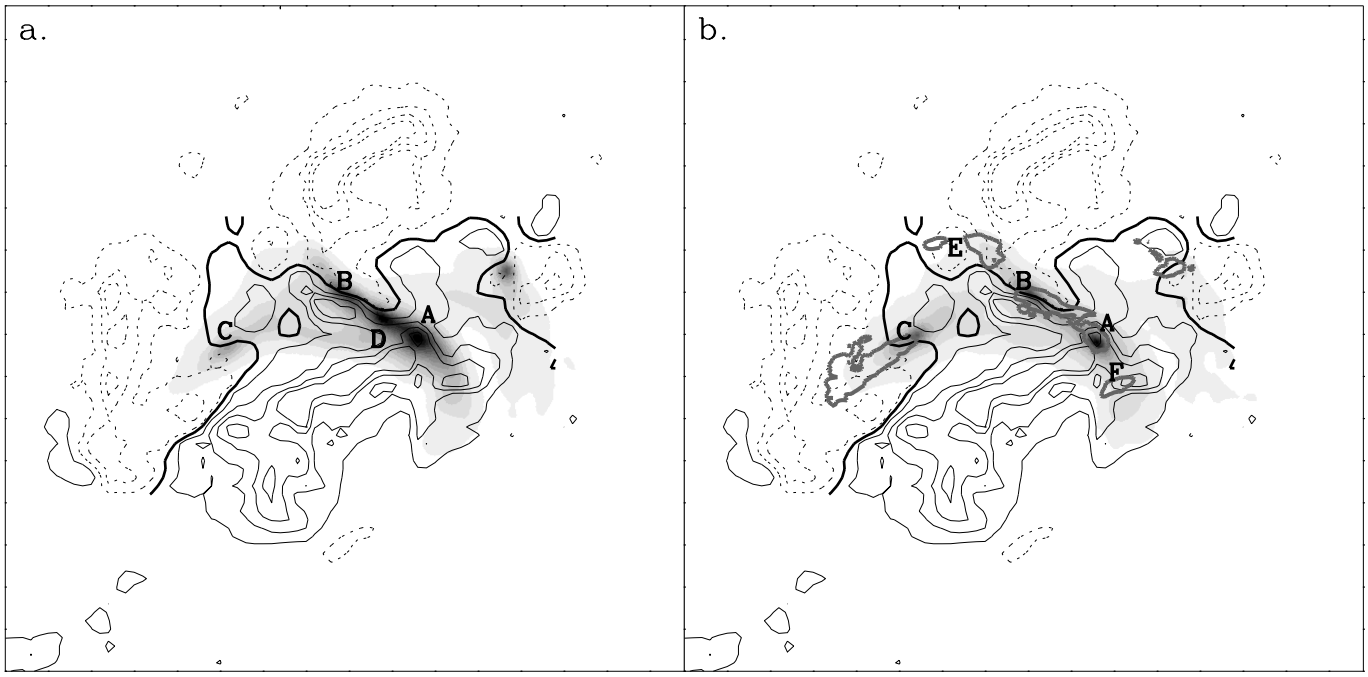

Fig. 3a and b. The magnetic longitudinal field (contours) on Oct. 27, 01:44UT superposed on the SXR images (grey map) on **a** Oct. 27, 01:44:33UT and **b** Oct. 27, 01:45:31UT taken by *Yohkoh* SXT from the filter Al.1. To illustrate clearly the structures at different times, the two SXR images are not shown in the same grey scale. The contour levels are the same as in Fig. 1. The thick dark line indicates the longitudinal field inversion line. In **b**, the H_β flare kernels (01:55:26UT on Oct. 27) are plotted in thick grey contours. The field of view (FOV) is $160'' \times 160''$.

be established, which may serve as a means to investigate the magnetic configuration in the space. Fig. 3 gives the coaligned observations of the flare in SXR and H_β images, superposed on the photospheric magnetogram taken on Oct. 27. The magnetic connection patterns are drawn in Fig. 4 and are found well identified with the flare regions.

A compact flaring loop (loop AB in Paper I) is prominently shown in the SXR images. Co-ordinated observations from other wavelengths show that A and B, the two ends of the loop, give compact HXR (up to 53keV) and H_α emissions, suggesting that they make the foot points of the SXR loop. The loop is well coaligned with the pattern L3, which emerged on this day along the magnetic inversion line M1. At the onset of the flare (Fig. 3a), three bright loci in SXR emission along this pattern seem to indicate the two emitting feet (A and B) and the bright top (D) of the L3 loop. Similarly, the magnetic connection pattern L2 finds its coronal counterpart in well coaligned SXR emission streak, which runs across the inversion line M2 and heads into an extended foot area (region C in Paper I) in S2 region. The co-alignment seen for this pattern also suggests that possibly L2 and L3 share a common foot which is foot A. For the pattern L1, the alignment of SXR emission even portrays the feature of the twist along this loop, which is rooted in E and F and seems to interact with the shorter loop L3 at the site of D. This point will be discussed in more details in Sect. 6. The coalignment in L4 just gives the last example in this comparison.

For all patterns, H_β emission is located at the ends of SXR streaks, or the footpoints of the loops in the chromosphere (seen in Fig. 3b). The above co-ordination is a comparison of the projections of the magnetic loop structure in the photosphere, chromosphere and corona, which offers an indirect way to view vividly the spatial configuration of the magnetic field, specifically, the magnetic structures associated with the energy storing, releasing or depositing sites where flares are produced.

5.2. Vertical current system and flares

In Fig. 4, we further demonstrate the spatial relationship between the flare regions and the vertical current distribution on October 27 when the flare occurred. It is seen that the feet of the flaring loop L3 in SXR are located immediately on the two sides of the current reverse line, which is virtually coaligned with the magnetic inversion line here (M1) (seen in Fig. 4a). One foot (A) is found just at the edge of the strong current concentration J_1^+, while the other (B) is almost above the reverse line of a current pair. However, the emergence of this bipole is continuously accompanied by the input of magnetic shear from below the photosphere, and the existence of horizontal current inside the loop L3 is probable.

The flaring loop L1 travels from the positive current concentration to the negative one, connecting the current pair of J_1^+-J_1^-, and the two feet E and F are well coaligned with it; one foot (E) is exactly located in the vertical current maximum of J_1^-, while the other one (F) is in between the maxima of two current concentrations J_1^+ and J_2^+ (seen in Fig. 4b). Since the magnetic field in the chromosphere and corona is generally regarded free from force (Metcalf et al. 1995), the pattern L1, given its long expanse, can be well extending to the corona and carrying the

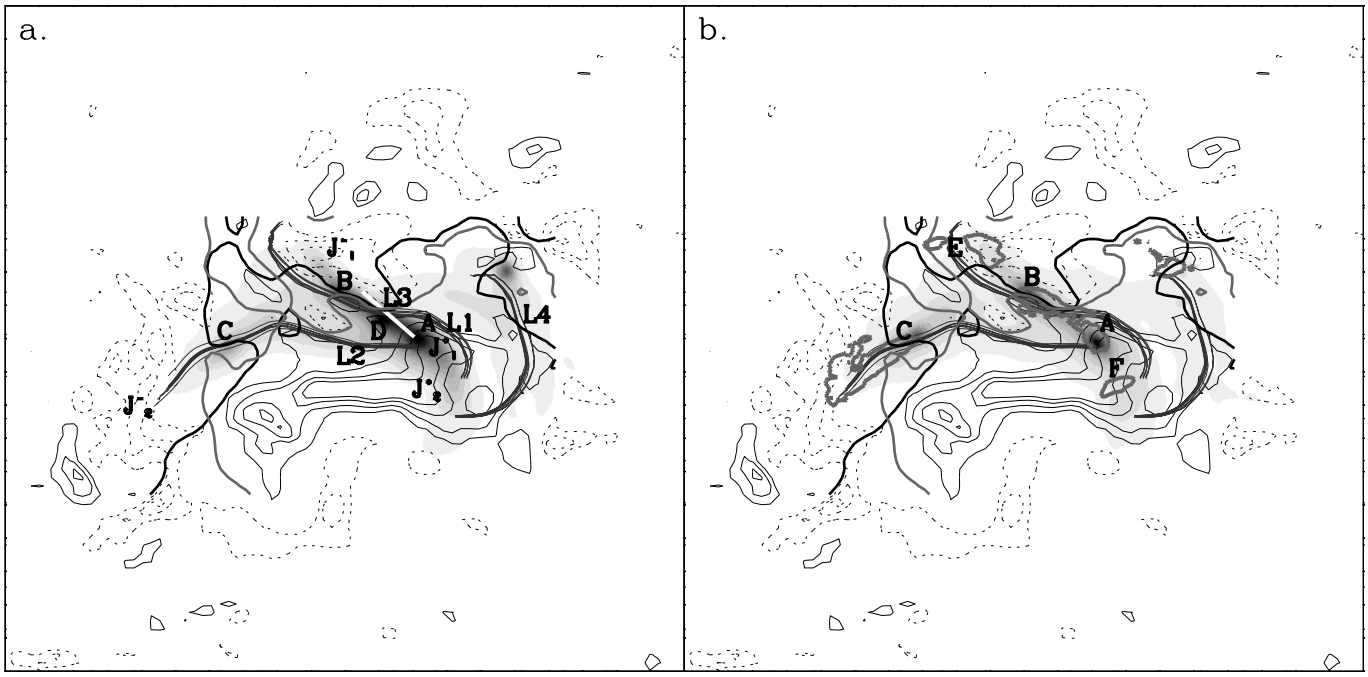

Fig. 4a and b. Coalignment of SXR images on **a** Oct. 27, 01:44:33UT, **b** Oct. 27, 01:45:31UT taken by *Yohkoh* SXT from the filter Al.1 with the vertical current distribution (contour) on Oct. 27, 01:44UT and with the magnetic connection patterns (thick grey curves). The white straight segment drawn by hand indicates L3 (see the text). The solid (dashed) lines represent the current flowing out of (into) the photosphere. The contour levels of both figures are $\pm$0.6, 1.2, 1.8, 2.4 $\times 10^{-2}$A/m^2. In both figures,the longitudinal inversion line is drawn in thick dark line and the current reverse line in thick grey line. In **b**, the H_β flare is overlapped in thick grey contours. The FOV is the same as that in Fig. 3.

field-aligned current whose footpoints are perched in the photosphere. The pattern L2 also straddles the vertical current reverse line around M2 from J_1^+ to J_2^-, but the site of C is not a region of strong current concentration.

The above comparison offers the information that the flare may originate from the instability at the interface between two current carrying loops, one being the pre-existing loop L1, and the other being the newly emerging and strongly sheared loop L3.

6. Discussions

Seen from Fig. 3a and Fig. 4a, at the onset of the flare, three bright regions were lying in the SXR emission streak along L3, among which, the feet regions A and B were further enhanced in the impulsive phase (Fig. 3b and Fig. 4b) and actually became the nonthermal electron depositing sites giving strong HXR and chromospheric features (Paper I), while the region D, or the top of loop L3, faded in the impulsive phase. The morphological comparison carried out in the previous sections seem to suggest that the interaction between L1 and L3 may occur at the site of D. Indeed, in Paper I, we have spotted a hot component of the coronal plasma and found that both thermal and nonthermal processes were taking place at the very onset of the flare; the HXR images synthesized from *Yohkoh* observation also reveal a loop top source at this time (Takakura et al. 1994). Combining the above facts, we are able to establish the following scenario of the initial phase of the flare: the flare was triggered by the interaction between two current-carrying loops at the top of loop L3 where the *in situ* energy release occurred through the rapidly heated plasma and energized electrons.

Fig. 5 illustrates the SXR flare at the onset of the event superposed on the map of free energy distribution. The concept of free energy used here is defined from the magnetic shear (Hagyard, Low, & Tandberg-Hanssen 1981), which is calculated as the following (Wang et al. 1996):

$$\rho_{free} = \frac{B_s^2}{8\pi} \quad (1)$$

where B_s is the source field (Hagyard, Low, & Tandberg-Hanssen 1981), or the departure of the observed vector field B_o from the potential field B_p deduced from the observed longitudinal field, B_s=B_o-B_p, which contains information on the path of atmospheric currents whose footpoints on the photosphere are mapped by vertical currents (Moreten & Severny 1968; Hagyard 1988; Wang et al. 1996)

It is seen that the flaring loop L3 is where the free energy gets most concentrated and the regions A, B and D are coaligned with the energy density maxima. To be more careful, since the loop L1 and L3 are fairly overlapped along the inversion line M1, we cannot tell definitely whether the free energy concentration is actually occurring along the interface between L1 and L3 or along the strongly sheared loop L3. Nevertheless, in either case, energy release in this flare should be taking place at the sites of free energy concentration (Machado et al. 1988; Low & Wolfson 1988). Particularly, one such site is the foot A, which is also the locus of the strong concentration of magnetic longi-

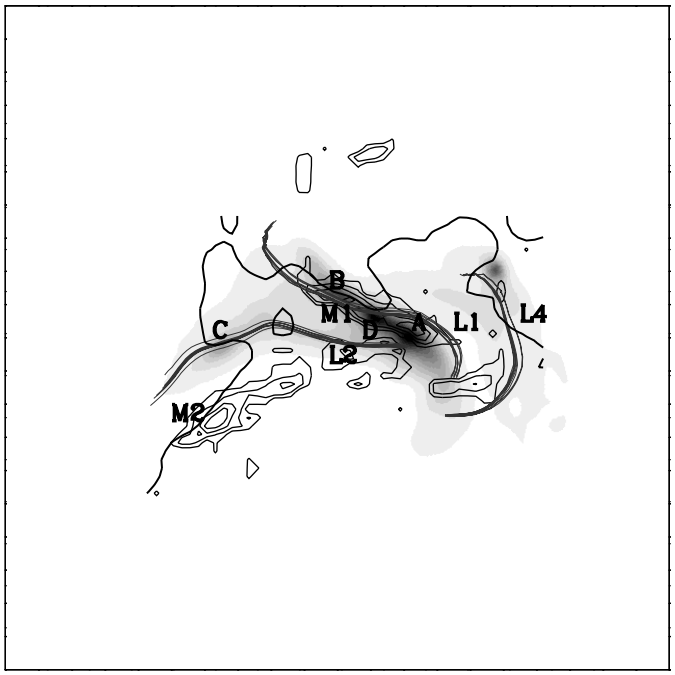

Fig. 5. The distribution of magnetic free energy (contour) superposed on the SXR image on Oct. 27, 01:44:33UT UT taken by *Yohkoh* SXT from the filter Al.1. The magnetic patterns are also shown in grey curves and the magnetic inversion line is draw in thick dark line. The contour levels are 1.5, 2.5, 3.8, 5.0 $\times 10^5$erg cm^{-3}. The FOV is the same as that in Fig. 3.

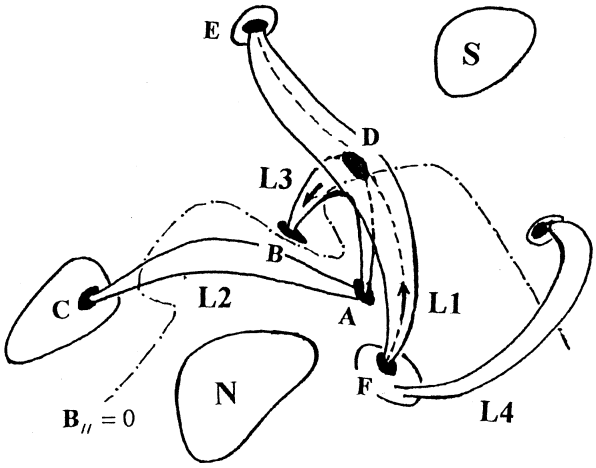

Fig. 6. The schematic interpretation of the flare configuration on Oct. 27.

tudinal flux, vertical current and free energy, and the other site is B, located over the reverse line of magnetic longitudinal field and vertical current, where strong non-potentiality is dominant and the separatrix layer may be involved in the energy release (Mandrini et al. 1995; Wang et al. 1997; Wang 1997).

A distinctly different case is seen for the pattern L2, which fairly deviate from the free energy concentration around M2, implying that the flaring of L2, unlike L3, could be a secondary effect of energy transfer from the initial flaring site. We are encouraged to hold that a certain energy flux from the flaring loop L3, was input along the loop L2 and impacted on region C, noting that the gradual radiative behavior and special H_α spectral feature in the region C support this idea (Paper I).

From above, a schematic interpretation of the trigger of energy release in the flare on October 27 is shown in the cartoon in Fig. 6.

7. Conclusion

In this paper, we investigate the evolution of the magnetic configuration in a famous active region (AR7321) from October 26 to October 27, just on the eve of the occurrence of a 1N/M1.1 flare. The vector photospheric magnetograms are exploited to recover the comprehensive magnetic connectivity patterns and the vertical current system, which are confirmed to bear close spatial correlation with the configuration of the flare observed in different wavelengths displaying the phenomenon from the chromospheric to the coronal level. With these results, we explore the magnetic configuration for the trigger and free energy release in the flare. Our main conclusions are summarized as follows:

The active region has continuous flux emergence which greatly enhanced nonpotentiality in this region; specifically, a newly emerging bipole on Oct. 27 along the inversion line brings in strong shear. This low-lying, strongly sheared loop (L3) pushes a pre-existent overlying loop (L1) and strong free energy is accumulated along this zone of magnetic complexity.

We employ the filtering technique on the observed raw photospheric magnetograms to obtain the vertical current distribution in this active region. It is found that the major current pairs were associated with the emerging flux. Some of the flare kernels show close spatial relationship to the strong current concentration sites. One loop (L1) can be approximately identified as carrying the field-aligned current with both feet rooted in the vertical current concentration sites; while the low-lying loop L3 straddles almost parallel to the magnetic inversion line and current reversing line. One end (A) of L3 was anchored on the edge of the vertical current maximum, and the other end (B) plunging into the reversing zone of longitudinal field and vertical current.

The magnetic connection patterns, deduced from the photospheric vector field, are identified in the space by the flare configuration in multi-waveband observations, and can thus be supposed as magnetic loops projected on the photosphere. We find clear evidence in the observations that the flare is initiated by the interaction between the two loops L3 and L1, on the top (D) of L3, and further energy release is triggered along the L3 loop, especially at the foot regions of A and B. All three bright loci seen in SXR images from the onset to the impulsive phase of the flare are well coaligned with the concentrations of the free magnetic energy, ie., the excess magnetic energy of the observed field to that of a potential field and the ways to release the free energy in these three regions may differ according to their local physics.

Subsequently, the flaring of another region (C) didn't go along the free energy concentration zone but appears a sec-

ondary effect from the initial flaring site (loop L3) through the transfer of energy flux. The above scenario of the flare is supported by the previous studies of the same event.

Acknowledgements. We would like to thank Prof. Wang J. for his valuable suggestions and discussions. One of us (QJ) thanks Dr. G. Roumeliotis who kindly offered the SXR deconvolving procedure IRIS (Roumeliotis 1995). We also thank Dr. T. Amari for commenting on the paper. This work is supported by the National Natural Science Foundation of China (NSFC), under grant 19791090 and 19403002.

References

Akioka M., Acton L.W., Hudson H.S., 1993, in: Proc. Yohkoh Science Meeting, ed. Y. Uchida, H.S. Hudson, K. Shibata and T. Watanabe (Tokyo Universal Academy Press), in Press
Canfield R.C., de La Beaujardiere J.-F., Fan Y., et al., 1993, ApJ 411, 362
Démoulin P., Hénoux J.C., Mandrini C.H., 1992, Solar Phys. 139, 105
Démoulin P., Mandrini C.H., Rovira M.G., Hénoux J.C., Machado M.E., 1994, Solar Phys. 150, 221
Fontenla J.M., Ambastha A., Kalman B., Csepura Gy., 1995, ApJ 440, 894
Hagyard M.J., 1988, Solar Phys. 115, 107
Hagyard M.J., 1990, Mem. Soc. Astron. Italia 61, 2, 337
Hagyard M.J., Rabin D.M., 1986, Adv. Space Res. 6(6), 7
Hagyard M.J., Low B.C., Tandberg-Hanssen E., 1981, Solar Phys. 73, 257
Hagyard M.J., Smith J.B., Jr. Teuber D., West E.A., 1984, Solar Phys. 91, 115
Hanaoka Y., 1996, Solar Phys. 165, 275
Kawakami S., 1993, in: Proc. the Second Japan-China Seminar on Solar Physics, ed. T. Sakurai, T. Hirayama and G. Ai, National Astronomical Observatory of Japan, p. 147
Kurokawa H., Kawai G., Kitai R., et al., 1992, PASJ 44, L129
Leka K.D., Canfield R.C., McClymont A.N., et al., 1993, ApJ 411, 370
Leka K.D., Canfield R.C., McClymont A.N., van Driel-Gesztelyi L., 1996, ApJ 462, 547
Lites B., Low B., Marting P.V., et al., 1995, ApJ 446, 877
Liu Y., Akioka M., Yan Y., Ai G., 1998, Solar Phys. 177, 395
Low B.C., Wolfson R., 1988, ApJ 324, 574
Machado M.E., Moore R.L., Hernandez A.M., et al., 1988, ApJ 326, 425
Mandrini C.H., Rovira M.G., Démoulin P., et al., 1993, A&A 27, 609
Mandrini C.H., Démoulin P., Rovira M.G., et al., 1995, A&A 303, 927
Mandrini C.H., Démoulin P., Van Driel-Gesztelyi L., et al., 1996, Solar Phys. 168, 115
Metcalf T.R., Jiao L., McClymont A.N., Canfield R.C., Uitenbroek H., 1995, ApJ 439, 474
Moore R.L., Hagyard M.J., Davis J.M., 1987, Solar Phys. 113, 347
Moreten G.E., Severny A.B., 1968, Solar Phys. 3, 282
Priest E.R., 1981, in: Solar Flares Magnetohydrodynamics, ed. E.R. Priest (New York: Gordon and Breach), p. 47
Qiu J., Wang T., Tang Y., Xu A., 1997, A&A, submitted
Roumeliotis G., 1995, ApJ 452, 495
Shi Z., Wang J., 1994, Solar Phys. 149, 105
Shi Z., Wang J., Wang H., 1995, Acta Astron. Sin. 36, 181
Takakura T., Nishio M., Nakajima H., et al., 1994, PASJ 46, 653
Tanaka K., 1991, Solar Phys. 136, 133
Wang J., 1994, Acta Astrophys. Sin., 34
Wang J., Shi Z., Wang H., Lü Y., 1996, ApJ 456, 861
Wang H.M., Tang F., 1993, ApJ 407, L89
Wang H.N., 1997, Solar Phys. 174, 265
Wang T., Xu A., Zhang H., 1994, Solar Phys. 155, 99
Wang T., Wang H.N., Qiu J., 1997, A&A, accepted
Zhang H., 1995, A&A 304, 541
Zhang H., Wang T., 1994, Solar Phys. 151, 129
Zirin H., 1983, ApJ 274, 900